

DOI:10.16410/j.issn1000-8365.2023.3003

一维量子反铁磁性材料研究简介

王艳红,符鹏,卢红成

(华中科技大学 化学与化工学院 湖北 武汉 430074)

摘要:低维量子磁性材料蕴含着丰富的磁性基态特点和量子相变行为,其低维结构与材料内部电子自旋耦合会产生诸多新奇的磁性能,在量子存储和量子传输等方面有着广泛的应用前景,近年来迅速成为研究前沿和热点。一维量子磁性材料由于结构简单,是研究低维量子磁性材料磁学性能的最佳体系,因而首先得到重点关注和研究。自物理学家Haldane教授提出具有整数和半整数自旋的一维量子反铁磁性材料具有不同的量子无序基态的猜想,研究者们对该类材料展示出极大兴趣,并在实验上不断得到了验证。本文简单介绍了部分具有不同自旋数的一维量子反铁磁性材料的制备方法、晶体结构及磁学性能等相关研究工作,为进一步实验合成更多新型一维量子磁性材料提供一定的依据和思路。

关键词:晶体结构;一维;量子磁性;自旋

中图分类号: TB34; O469

文献标识码:A

文章编号:1000-8365(2023)01-0015-08

Brief Introduction of One-Dimensional Quantum Antiferromagnetic Materials

WANG Yanhong, FU Peng, LU Hongcheng

(School of Chemistry and Chemical Engineering, Huazhong University of Science and Technology, Wuhan 430074, China)

Abstract: Low-dimensional quantum magnetic materials have rich magnetic ground states and quantum phase transition behaviors. Their low-dimensional structure and internal electronic spin coupling could exhibit rich novel magnetic properties, which have wide application prospects in quantum storage and quantum transmission and have rapidly become the research frontier and hot topic in recent years. Because of their simple structures, one-dimensional quantum magnetic materials are the best systems to study the magnetic properties of low-dimensional quantum magnetic materials and thus have been focused on and studied first. Since the physicist Professor Haldane conjectured that one-dimensional quantum antiferromagnetic materials with integer and semi-integer spins have different quantum disordered ground states, researchers have been greatly interested in these materials, which have been continuously verified by experiments. In this paper, the preparation methods, crystal structure and magnetic properties of some one-dimensional quantum antiferromagnetic materials with different spin numbers are briefly introduced and provide some ideas and methods to experimentally synthesize more new one-dimensional quantum magnetic materials.

Key words: crystal structure; one-dimensional; quantum magnetism; spin

在传统三维磁性材料中,随着温度的降低,热运动逐渐减弱,材料的磁性通常会在某个临界温度(居里温度 T_c 或尼尔温度 T_N)发生磁相变,达到经典的三维长程磁有序(铁磁或反铁磁有序)。而对于低维量子磁性材料,由于反铁磁性、低维性以及小自旋等因素,具有强烈的量子自旋涨落,使得其自旋在温度很低、甚至绝对零度下都能避免三维长程磁有序的出现,其基态一直处于自旋强纠缠下的高简并

无序态,从而呈现出量子自旋液体、自旋轨道分离^[1-4]、自旋能隙态^[5-7]、spin-Peierls相变^[8-10]、波色-爱因斯坦(Bose-Einstein)相变^[11-13]、磁化台阶^[14-16]等丰富有趣的新奇量子现象。同时,由于低维量子磁性材料具有一维链或二维平面的结构特征,其自旋量子涨落与同样具有低维结构的铜基、铁基等非常规高温超导化合物的超导电性有很强的关联性^[17-18],在理解和解释超导机理方面也有着非常重要的科学意义。此外,低

收稿日期:2023-01-12

基金项目:国家自然科学基金(21901078)

作者简介:王艳红,1994年生,博士生。研究方向:一维量子磁性材料的研究。电话:15073029319,Email:d202080179@hust.edu.cn

通讯作者:卢红成,1987年生,博士,研究员。研究方向:低维量子磁性材料等功能晶体材料的研究。Email:hcl@hust.edu.cn

引用格式:王艳红,符鹏,卢红成.一维量子反铁磁性材料研究简介[J].铸造技术,2023,44(1): 15-22.

WANG Y H, FU P, LU H C. Brief introduction of one-dimensional quantum antiferromagnetic materials [J]. Foundry Technology, 2023, 44(1): 15-22.

维量子磁性材料可以产生满足非对易统计、有能隙的分数化自旋激发，并且这种激发受长程量子纠缠的保护，使其不受局部微扰和噪声的影响，在容错拓扑量子计算、量子存储和量子传输等方面有广泛的应用前景^[19-20]，是实现量子计算实用化的途径之一。因此，低维量子磁性材料因具有量子自旋液体和自旋轨道分离等丰富有趣的新奇量子现象，与非常规高温超导的相关性以及在量子计算、量子存储和量子传输等方面的应用前景，引起了人们的极大关注，迅速成为研究前沿和热点^[21-30]。

一维量子反铁磁性材料磁性相对较简单，因此首先得到重点关注和研究。不同于链内和主磁交换作用均为铁磁性的单链磁体，一维量子反铁磁性材料的链内磁交换作用 J 为反铁磁性作用，可以产生强烈的量子自旋涨落，从而具有量子自旋液体等新奇量子现象。2016 年，诺贝尔物理学奖获得者 Haldane 教授曾提出一个著名的猜想^[31]：半整数自旋($S=1/2, 3/2, 5/2 \dots$)和整数自旋($S=1, 2, 3 \dots$)一维量子反铁磁性链系统分别具有不同的量子无序基态。当自旋为半整数时，自旋链系统低能激发无能隙，但可能存在 spin-Peierls 相变，自旋—自旋两点间的关联函数随距离呈幂律形式衰减；当自旋为整数时，自旋链系统呈现出具有能隙的自旋单态，自旋—自旋两点间的关联函数随距离呈指数形式衰减。随着研究的不断深入，Haldane 猜想很快得到了实验验证。Haldane 猜想的正确性改变了人们认为半整数自旋与整数自旋一维量子反铁磁性链情形完全相同的传统看法，使许多科研工作者对一维量子反铁磁性链体系的研究产生了极大的兴趣^[32]。本文主要介绍了部分具有半整数和整数自旋的经典一维量子反铁磁性材料的制备方法、晶体结构及其磁性能。

1 半整数自旋一维量子反铁磁性材料

根据 Haldane 猜想，具有半整数自旋的一维量子反铁磁性材料可能具有 spin-Peierls 相变。目前研

究较多的具有半整数自旋的一维量子反铁磁性化合物主要包括 TTF-MS₄C₄(CF₃)₄ (TTF=四硫富瓦烯；M=Cu²⁺,Au²⁺)^[33-35]、CuGeO₃^[36]、BaCu₂Si₂O₇^[37]、Cu₃(CO₃)₂(OH)₂^[38] 等，其中化合物 TTF-MS₄C₄(CF₃)₄ (M=Cu²⁺,Au²⁺) 和 CuGeO₃ 被发现存在 spin-Peierls 相变，化合物 BaCu₂Si₂O₇ 存在自旋偏转相变，化合物 Cu₃(CO₃)₂(OH)₂ 被发现具有 1/3 磁化平台，而化合物 BaMn₂V₂O₈ 被发现可能表现出经典磁性行为与量子磁性行为并存的现象。下面依次进行简单介绍。

化合物 TTF-MS₄C₄(CF₃)₄ (M=Cu²⁺, Au²⁺) 最早被发现存在 spin-Peierls 相变^[33,35]。2 个化合物均通过在乙腈溶液中缓慢冷却得到。TTF-CuS₄C₄(CF₃)₄ 与 TTF-AuS₄C₄(CF₃)₄ 具有相同结构，均结晶于三斜晶系，空间群为 P-1(图 1)。在其结构中，MS₄C₄(CF₃)₄ 阴离子通过超交换相互作用沿 c 轴形成一维磁性链^[34]。如图 2 所示，TTF-CuS₄C₄(CF₃)₄ 与 TTF-AuS₄C₄(CF₃)₄ 的磁化率分别在温度低于 12 K 和 2.1 K 时急剧下降，表明这 2 种化合物在相应温度发生了 spin-Peierls 相变。此时该链系统发生自旋晶格二聚化转变，单重基态与三重激发态分开，从而产生自旋能隙，体系经过相变后处于具有自旋能隙的非磁性基态^[39]。

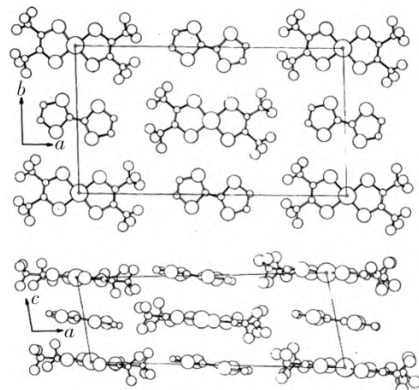


图 1 TTF-CuS₄C₄(CF₃)₄ 在 ab 和 ac 面上的晶体结构示意图^[33]
Fig.1 The crystal structure of TTF-CuS₄C₄(CF₃)₄ viewed on the ab-plane and the ac-plane^[33]

CuGeO₃ 是首个被发现具有 spin-Peierls 相变的无机化合物^[8,36]，打破了科研工作者对 spin-Peierls 相

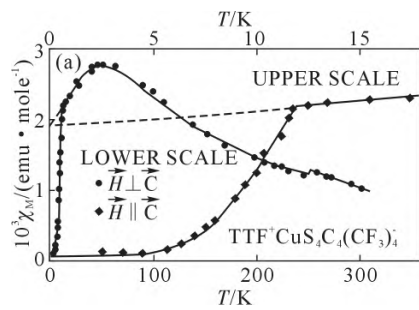
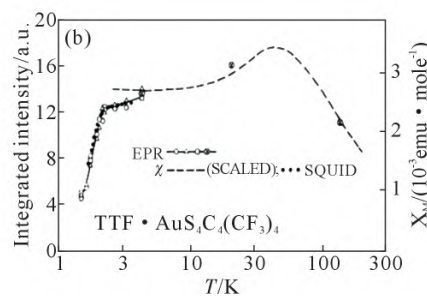


图 2 磁化率随温度变化曲线：(a) TTF-CuS₄C₄(CF₃)₄，(b) TTF-AuS₄C₄(CF₃)₄^[35]
Fig.2 Temperature dependence of magnetic susceptibilities: (a) TTF-CuS₄C₄(CF₃)₄, (b) TTF-AuS₄C₄(CF₃)₄^[35]



变在有机化合物中独有的认识,引起了科学界的轰动^[40-44]。该化合物最早由 Völlenkle 等^[45]通过在铂坩埚中高温烧结的方法合成得到。 CuGeO_3 结晶于正交晶系,空间群为 $Pbmm$ 。常温下, Cu^{2+} 与 4 个氧原子配位形成 CuO_4 平面, CuO_4 基团通过共边连接沿 c 轴延伸形成线性自旋链^[45]。如图 3(a)所示,当温度降至 14 K 时, CuGeO_3 的结构发生了变化, GeO_6 八面体角上的 $\text{O}_1\text{-O}_2$ 发生扭曲,变为四面体, Cu^{2+} 之间最近邻距离由 2.942 Å 变为 2.926 Å^[46]。磁化率随温

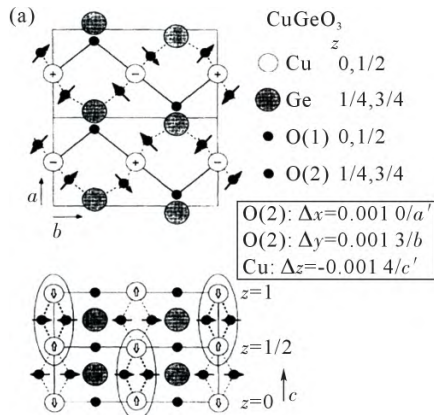


图 3 CuGeO_3 的性质:(a) 低温 spin-Peierls 相的结构示意图,(b) 在 $H=1 \text{ T}$ 外场下单晶样品的磁化率随温度变化曲线^[46,51]
Fig.3 The properties of CuGeO_3 : (a) schematic representation of the low-temperature structure in the spin-Peierls state, (b) temperature dependence of magnetic susceptibility for a single-crystal measured under $H=1 \text{ T}$ ^[46,51]

型化合物^[37,54-61]。该化合物最早由 Tsukada 等^[54]通过常规固相反应得到,并使用浮区法生长出直径为 5 mm,长度为 10 mm 的单晶棒样品。在 $\text{BaCu}_2\text{Si}_2\text{O}_7$ 中, CuO_4 平面通过 O 原子以角连接的方式连接形成沿 c 轴的一维自旋链(图 4)。如图 5 所示^[37],对 $\text{BaCu}_2\text{Si}_2\text{O}_7$ 外加一个沿 c 轴方向的磁场,随着磁场强度的增加, $\text{BaCu}_2\text{Si}_2\text{O}_7$ 的磁化强度线性增加。当 $H=2.0 \text{ T}$ 时,自旋发生偏转,磁化强度出现跳跃,体系的反铁磁相被破坏,形成了 spin-flop1 相。之后磁化强度继续随着场强增加而线性增加,直至 4.9 T 时再次出现跳跃,体系进入 spin-flop2 相。

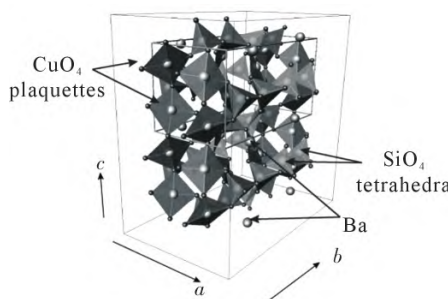


图 4 $\text{BaCu}_2\text{Si}_2\text{O}_7$ 的晶体结构图^[54]
Fig.4 The crystal structure of $\text{BaCu}_2\text{Si}_2\text{O}_7$ ^[54]

具有 1/3 磁化平台的一维金刚石链化合物 $\text{Cu}_3(\text{CO}_3)_2(\text{OH})_2$ 为天然矿物蓝铜矿,在此不再描述其合成方法。该化合物结晶于单斜晶系,空间群为 $P2_1/c$ ^[62]。

度变化的曲线显示当温度低于 14 K 时,磁化率在 3 个晶轴方向上都出现了急剧下降,体系发生 spin-Peierls 相变,形成二聚化的自旋能隙基态^[47-52](图 3(b))。有趣的是,Li 等^[53]研究发现 CuGeO_3 的尺寸和形貌与其 spin-Peierls 相变之间存在着一定的关系。当 CuGeO_3 为纳米棒且长度小于 600 nm 时不存在 spin-Peierls 相变,而在长度大于 600 nm 的纳米线中则可以出现较弱的 spin-Peierls 相变。

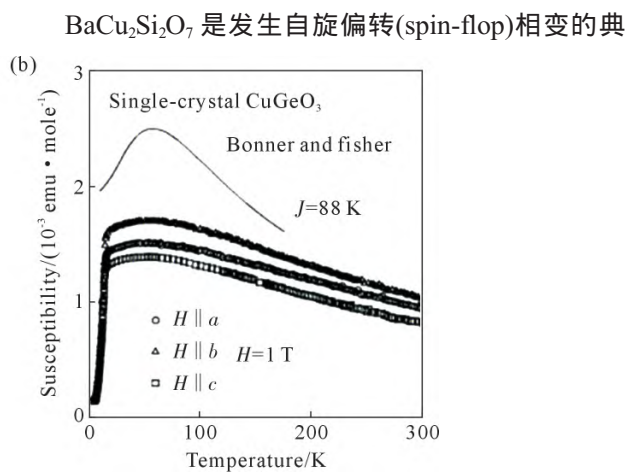


图 3 CuGeO_3 的性质:(a) 低温 spin-Peierls 相的结构示意图,(b) 在 $H=1 \text{ T}$ 外场下单晶样品的磁化率随温度变化曲线^[46,51]
Fig.3 The properties of CuGeO_3 : (a) schematic representation of the low-temperature structure in the spin-Peierls state, (b) temperature dependence of magnetic susceptibility for a single-crystal measured under $H=1 \text{ T}$ ^[46,51]

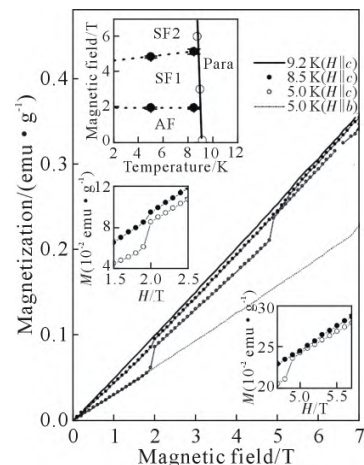
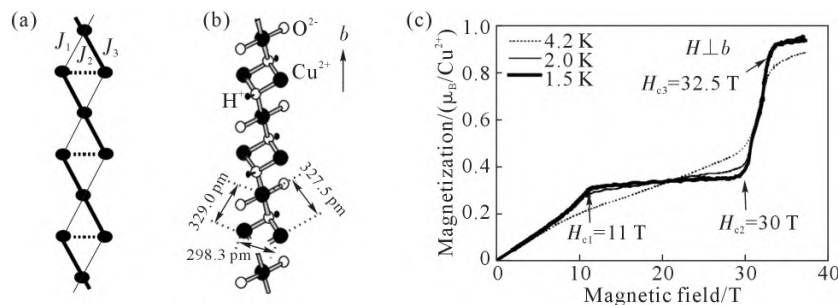


图 5 $\text{BaCu}_2\text{Si}_2\text{O}_7$ 的磁化强度随外加磁场变化曲线^[37]
Fig.5 Field dependence of the magnetization for $\text{BaCu}_2\text{Si}_2\text{O}_7$ ^[37]

如图 6(b)所示,自旋为 $S=1/2$ 的磁性金属 Cu^{2+} 通过 O 原子以角共享的方式连接,从而形成沿 b 轴无限延伸的一维磁性链。在磁性链中存在 J_1 、 J_2 和 J_3 3 种自旋耦合交换作用,由于 $J_2 \gg J_1, J_3$,因此 J_1 和 J_3 可以忽略不计(图 6(a))。图 6(c)为 $\text{Cu}_3(\text{CO}_3)_2(\text{OH})_2$ 的等温磁化强度随磁场变化曲线。在低场处,化合物的磁化强度随着外加磁场的增大而线性增加,直至 $H=11 \text{ T}$ 时,产生 J_2 自旋耦合交换作用的 2 个 Cu^{2+} 离子的自旋发生二聚化耦合,磁矩相互抵消,宏观上只表现出第三个 Cu^{2+} 离子自旋的磁矩,导致磁化强

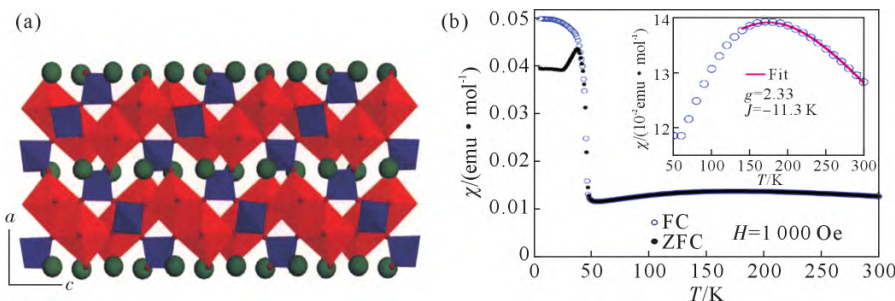
图 6 $\text{Cu}_3(\text{CO}_3)_2(\text{OH})_2$ 的性质:(a) 金刚石链结构,(b)晶体结构示意图,(c)高场磁化强度曲线^[62]Fig.6 The properties of $\text{Cu}_3(\text{CO}_3)_2(\text{OH})_2$: (a) the diamond chain, (b) the crystal structure, (c) the high-field magnetization curves^[62]

度随磁场变化曲线在 $H=11\sim30$ T 时出现一个 $1/3$ 平台。随着磁场继续增大,相互抵消的磁矩被破坏掉,总磁矩迅速达到饱和。Kikuchi 等^[63]测量了其高场磁化率和 ^1H NMR,发现该化合物的基态处于无能隙相。此外,Kamikawa 等^[64]通过高场电子顺磁共振测试发现该化合物在 20 K 以下观察到朗德因子 g 的位移,与磁化率曲线的变化一致。

$\text{BaMn}_2\text{V}_2\text{O}_8$ 因具有大自旋的金属磁性离子 $\text{Mn}^{2+}(S=5/2)$,其基态磁性有可能表现出经典磁性行为与量子磁性行为并存的现象,引起了科研工作者的极大兴趣^[38]。如图 7(a)所示, $\text{BaMn}_2\text{V}_2\text{O}_8$ 结晶于四方晶系, Mn^{2+} 与 6 个 O 原子配位形成 MnO_6 八面体, Mn^{2+} 位于 MnO_6 八面体的中心。 MnO_6 八面体通过共边的连接方式沿着 c 轴延伸形成无限长的螺旋磁性链,链与链之间由碱土金属 Ba^{2+} 和 VO_4 四面体隔开。磁化率随温度变化的曲线表明, $\text{BaMn}_2\text{V}_2\text{O}_8$ 的磁化率在 170 K 左右形成了宽峰,是低维磁性化合物的典型特征,表明在该温度下化合物存在短程磁有序(图 7(b))。在 37 K 时,磁化率随温度变化曲线出现典型的 λ 型尖峰,表明 $\text{BaMn}_2\text{V}_2\text{O}_8$ 出现了反铁磁性有序转变。Pal 等^[65]通过温度依赖的拉曼光谱发现该化合物在奈尔温度以下至少存在 2 种声子模式,在奈尔温度以上拉曼模式发生异常热演化,该现象与短程磁有序有关。

2 整数自旋一维量子反铁磁性材料

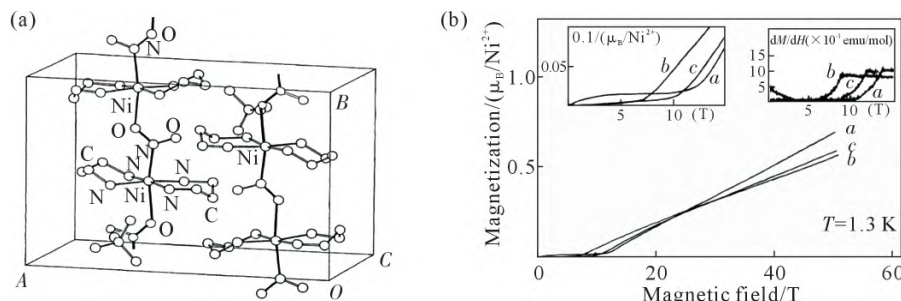
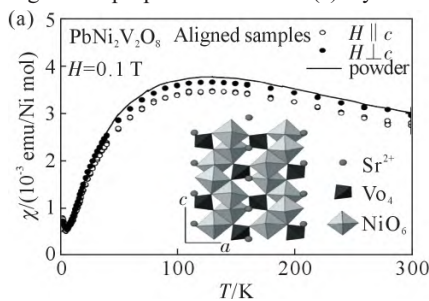
与具有半整数自旋的一维量子反铁磁性材料不

图 7 $\text{BaMn}_2\text{V}_2\text{O}_8$ 的性质;(a) $\text{BaMn}_2\text{V}_2\text{O}_8$ 的晶体结构,(b) $\text{BaMn}_2\text{V}_2\text{O}_8$ 的磁化率随温度变化曲线^[38]Fig.7 The properties of $\text{BaMn}_2\text{V}_2\text{O}_8$: (a) the crystal structure of $\text{BaMn}_2\text{V}_2\text{O}_8$, (b) temperature dependence of magnetic susceptibility for $\text{BaMn}_2\text{V}_2\text{O}_8$ ^[38]

同,具有整数自旋的一维量子反铁磁性材料在其基态和激发态之间存在着有限能隙,该能隙又可以被称为 Haldane 能隙。目前,该能隙在很多 $S=1$ 的化合物中被测得,如 $\text{Ni}(\text{C}_3\text{H}_8\text{N}_2)_2\text{NO}_2\text{ClO}_4$ (NENP)^[66-68], $\text{SrNi}_2\text{V}_2\text{O}_8$ ^[69-71], RbNiCl_3 ^[72], R_2BaNiO_5 (R 为 Y 或稀土元素)^[73-74]。研究较多的具有整数自旋的一维量子反铁磁性化合物主要包括 NENP^[66-68]、 $\text{ANi}_2\text{V}_2\text{O}_8$ ($\text{A}=\text{Sr}^{2+}$, Pb^{2+})^[69-71]、 $\text{MnCl}_3(2,2'-\text{bpy})$ ^[75]等,依次简单介绍如下。

NENP 是首个被发现存在 Haldane 能隙的化合物^[68]。该化合物的单晶样品是通过在水溶液中缓慢挥发得到^[76]。如图 8(a)所示,Ni 原子在 ac 平面内与 2 个二甲胺的 4 个 N 原子配位。在 b 轴方向上,Ni 原子通过亚硝酸根离子连接形成无限长的一维磁性链。高氯酸根离子填充在链与链之间,将磁性链隔开。图 8(b)表明,NENP 的磁化强度在低场时基本为 0,当外加磁场增加至 7.5 T 时,磁化强度开始呈直线上升,证实了 Haldane 能隙的存在。

$\text{PbNi}_2\text{V}_2\text{O}_8$ ^[7]是通过传统的固相合成方法制备得到,在室温时属于四方晶系,空间群为 $I4_{1}cd$,晶胞参数为 $a=12.1617$ Å 和 $c=8.3247$ Å。如图 9(a)所示, $\text{PbNi}_2\text{V}_2\text{O}_8$ 中 NiO_6 八面体沿 c 轴方向通过共边连接形成一维磁性链,链与链之间通过 VO_4 四面体隔开,而 Sr^{2+} 填充在金属链周围。磁化率随温度变化曲线表明该化合物在 120 K 时出现一个宽峰,随后磁化率迅速下降,在低温时随温度下降而上升,没有达到三维长程磁有序。对磁化率进行分析可以得到热

图 8 NENP 的性质:(a) 晶体结构,(b) 磁化强度随磁场变化曲线^[68]Fig.8 The properties of NENP: (a) crystal structure, (b) field dependence of the magnetization^[68]图 9 PbNi₂V₂O₈ 的磁性能:(a) 磁化率随温度变化曲线Fig.9 Magnetic properties of PbNi₂V₂O₈: (a) temperature dependence of magnetic susceptibility, (b) field dependence of the magnetization^[7]

激活能 $\Delta=29.4 \text{ K}$ ($H \parallel c$) 和 $\Delta=27.8 \text{ K}$ ($H \perp c$)。此外, 图 9(b) 中磁化强度随磁场变化曲线的斜率发生了明显改变, 表明存在磁相变, Haldane 能隙在临界场附近先闭合再打开。Hashi 等^[77]在 30 T 时对该化合物进行了⁵¹V 核磁共振测试, 发现该化合物的核磁谱图在 12 K 处开始分裂, 表明在该温度时出现了反铁磁有序。

Pahari 等^[69]发现与 PbNi₂V₂O₈ 结构相同的 SrNi₂V₂O₈ 在温度低至 3.75 K 时也未表现出长程磁有序, 与非弹性中子散射实验的结果相符合。研究表明其 Haldane 能隙约为 25 K, 基态呈自旋液态, 并进一步揭示了其在 3.7~300.0 K 的温度范围内为反铁磁性相互作用。

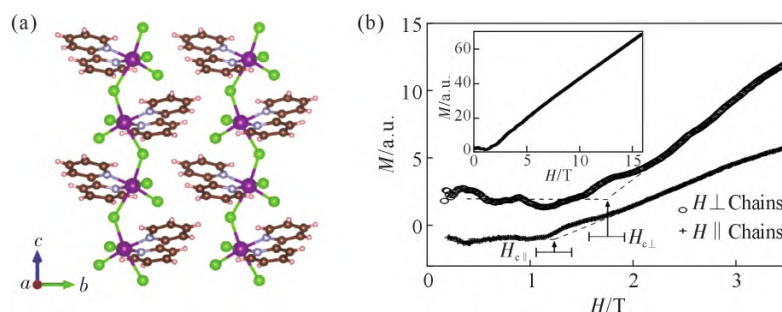
自旋为 $S=2$ 的 MnCl₃(2,2-bpy)最初被认为是唯一一个在大自旋体系中实现 Haldane gap 的化合物^[75], 由常温挥发的方法制备得到^[78]。该化合物以 Mn 为中心, 与 2,2'-bpy 的 2 个 N 原子和 4 个 Cl 原子配位形成 MnN₂Cl₄ 八面体。MnN₂Cl₄ 八面体以 Cl

原子作为桥联原子通过角连接的方式沿 c 轴形成一维自旋链, 链内 $\angle \text{Mn}-\text{Cl}-\text{Mn}$ 为 135°, 表现出反铁磁性相互作用。链与链之间通过有机分子 2,2'-bpy 和氢键相隔开, 使链间磁性金属 Mn 的最近邻距离增大到 7.96 Å, 从而实现较弱的链间磁相互作用。如图 10(b)所示, 30 mK 下 MnCl₃(2,2-bpy)的磁化强度在低场时基本为 0, 直至 $H=1.2 \text{ T}$ ($H \parallel c$) 和 $H=1.8 \text{ T}$ ($H \perp c$) 时, 磁化强度开始上升, 表明该化合物存在 Haldane 能隙^[75]。

然而在后续的研究中, Hagiwara 等^[79]测量了 MnCl₃(2,2-bpy)单晶沿 b 轴方向的磁化率随温度变化的曲线, 结果显示化合物的磁化率在 11 K 左右形成了尖锐的 λ 型峰, 表明 MnCl₃(2,2-bpy)在 11 K 出现了反铁磁有序转变(图 11)。

3 总结和展望

目前, 通过各种实验方法合成得到的一维量子反铁磁性材料数量较多, 但可以表现出新奇磁性性

图 10 MnCl₃(2,2-bpy)的性质:(a) 晶体结构,(b) 磁化强度随磁场变化曲线^[75]Fig.10 The properties of MnCl₃(2,2-bpy): (a) crystal structure, (b) field dependence of the magnetization^[75]

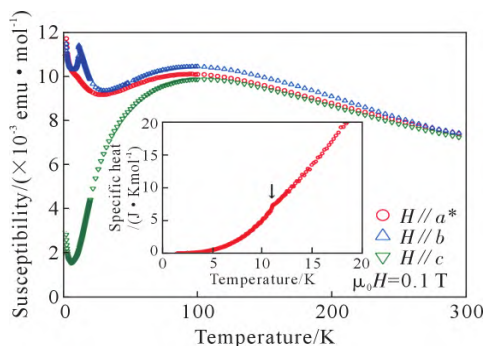


图 11 $\text{MnCl}_3(2,2\text{-bpy})$ 沿 a , b 和 c 轴的磁化率随温度变化
曲线^[79]

Fig.11 Temperature dependence of magnetic susceptibilities for $\text{MnCl}_3(2,2\text{-bpy})$ along the a , b and c axes^[79]

能的一维量子反铁磁性材料较少。此外，在大自旋体系中能实现 Haldane 能隙的化合物基本没有。因此，在今后对一维量子反铁磁性材料的研究中需要合成更多更优异的模型，为人们进一步理解一维量子反铁磁性材料的本质、新奇量子现象的起源、超导现象的解释及后续的实际应用提供实验材料。

参考文献：

- [1] BALENT S L. Spin liquids in frustrated magnets[J]. Nature, 2010, 464: 199-208.
- [2] 冉柯静, 王靖珲, 温锦生. 通往量子自旋液体的新路径——Kitaev 模型的材料实现[J]. 物理, 2021, 50(7): 443-453.
RAN K J, WANG J H, WEN J S. A new route to quantum spin liquids: Material realization of the Kitaev model[J]. Physics, 2021, 50 (7): 443-453.
- [3] DU L J, HUANG Y, WANG Y M, et al. 2D proximate quantum spin liquid state in atomic-thin α -RuCl₃[J]. 2D Materials, 2019, 6 (1): 015014.
- [4] LI Y S, CHEN G, TONG W, et al. Rare-earth triangular lattice spin liquid: A single-crystal study of YbMgGaO₄[J]. Physical Review Letters, 2015, 115: 167203.
- [5] HE Z Z, TANIYAMA T, KYÔMEN T, et al. Field-induced order-disorder transition in the quasi-one-dimensional anisotropic antiferromagnet BaCo₂V₂O₈[J]. Physical Review B, 2005, 72: 172403.
- [6] MENTRE O, DHAUSSY A C, ABRAHAM F, et al. Structural, infrared, and magnetic characterization of the solid solution series Sr_{2x}Pb_x(VO)(VO₄)₂: evidence of the Pb²⁺ 6s² lone pair stereochemical effect[J]. Journal of Solid State Chemistry, 1998, 140(2): 417-427.
- [7] UCHIYAMA Y, SASAGO Y, TSUKADA I, et al. Spin-vacancy-induced long-range order in a new haldane-gap antiferromagnet [J]. Physical Review Letters, 1999, 83: 632-635.
- [8] HASE M, TERASAKI I, UCHINOKURA K. Observation of the spin-Peierls transition in linear Cu²⁺(spin-1/2) chains in an inorganic compound CuGeO₃[J]. Physical Review Letters, 1993, 70(23): 3651-3654.
- [9] HASE M, TERASAKI I, UCHINOKURA K, et al. Magnetic phase diagram of the spin-Peierls cuprate CuGeO₃[J]. Physical Review B, 1993, 48: 9616-9619.
- [10] 卢蒙蒙, 陈斌. 含阻挫和各向异性的反铁磁自旋链的键算符理论[J]. 上海理工大学学报, 2020, 42(6): 607-611.
LU M M, CHEN B. Bond operator theory of antiferromagnetic spin chain with bond alternation and anisotropy[J]. Journal of University of Shanghai for Science and Technology, 2020, 42 (6): 607-611.
- [11] KUDO K, YAMAZAKI M, KAWAMATA T, et al. Drastic enhancement of thermal conductivity in the Bose-Einstein condensed state of TlCuCl₃[J]. Journal of the Physical Society of Japan, 2004, 73: 2358-2361.
- [12] NIKUNI T, OSHIKAWA M, OOSAWA A, et al. Bose-Einstein condensation of dilute magnons in TlCuCl₃[J]. Physical Review Letters, 2000, 84: 5868-5871.
- [13] RADU T, WILHELM H, YUSHANKHAI V, et al. Bose-Einstein condensation of magnons in Cs₂CuCl₄[J]. Physical Review Letters, 2005, 95(12): 127202.
- [14] KAGEYAMA H, YOSHIMURA K, STERN R, et al. Exact dimer ground state and quantized magnetization plateaus in the two-dimensional spin system SrCu₂(BO₃)₂[J]. Physical Review Letters, 1999, 82: 3168-3171.
- [15] KIKUCHI H, FUJII Y, CHIBA M, et al. Experimental observation of the 1/3 magnetization plateau in the diamond-chain compound Cu₃(CO₃)₂(OH)₂[J]. Physical Review Letters, 2005, 94: 227201.
- [16] MATSUMOTO M. Microscopic model for the magnetization plateaus in NH₄CuCl₃[J]. Physical Review B, 2003, 68, 180403.
- [17] CHEN R Y, WANG N L. Progress in Cr- and Mn-based superconductors: A key issues review[J]. Reports on Progress in Physics, 2019, 82: 012503.
- [18] WANG D F, KONG L Y, FAN P, et al. Evidence for Majorana bound states in an iron-based superconductor[J]. Science, 2018, 362(6412): 333-335.
- [19] KITAEV A. Anyons in an exactly solved model and beyond[J]. Annals of Physics, 2006, 321(1): 2-111.
- [20] KITAEV A Y. Fault-tolerant quantum computation by anyons[J]. Annals of Physics, 2003, 303(1): 2-30.
- [21] AHAMI N, BAZ M E. Thermal entanglement in a mixed spin Heisenberg XXX chain with DM interaction[J]. International Journal of Quantum Information, 2021, 19(5): 2150021.
- [22] GNANA BLESSY B S, LATHA M M. Chaotic dynamics of Heisenberg ferromagnetic spin chain with bilinear and biquadratic interactions[J]. Physica B: Condensed Matter, 2017, 523: 114-124.
- [23] GNANA BLESSY B S, LATHA M M. A chaotic study on Heisenberg ferromagnetic spin chain using Dzyaloshinski-Moriya interactions[J]. Pramana, 2019, 93: 70.
- [24] GUARNACCIA G, NOCE C. Quantum disordered vector-spin-chirality state in one dimensional Heisenberg model[J]. European Physical Journal B, 2019, 92: 212.
- [25] HANN C T, HUFFMAN E, CHANDRASEKHARAN S. Solution to the sign problem in a frustrated quantum impurity model[J]. Annals of Physics, 2017, 376: 63-75.
- [26] KRUPNITSKA O. Frustrated quantum Heisenberg double-tetrahedral and octahedral chains at high magnetic fields[J]. Physical Review B, 2020, 102: 064403.

- [27] LI N B. Energy and spin diffusion in the one-dimensional classical Heisenberg spin chain at finite and infinite temperatures[J]. Physical Review E, 2019, 100: 062104.
- [28] POPKOV V, SCHÜTZ G M. Solution of the Lindblad equation for spin helix states[J]. Physical Review E, 2017, 95: 042128.
- [29] ROJAS O. A conjecture on the relationship between critical residual entropy and finite temperature pseudo-transitions of one-dimensional models[J]. Brazilian Journal of Physics, 2020, 50: 675-686.
- [30] TORLAI G, MCALPINE K D, CHIARA G D. Schmidt gap in random spin chains[J]. Physical Review B, 2018, 98: 085153.
- [31] HALDANE F D M. Nonlinear field theory of large-spin Heisenberg antiferromagnets: Semiclassically quantized solitons of the one-dimensional easy-axis Néel state[J]. Physical Review Letters, 1983, 50: 1153-1156.
- [32] 张广铭. 物理诺奖之 Haldane 相的来龙去脉[J]. 物理, 2016, 45(12): 769-773.
ZHANG G M. The origin of the Haldane gapped phase[J]. Physics, 2016, 45(12): 769-773.
- [33] BRAY J W, HART H R, INTERRANTE L V, et al. Observation of a spin-Peierls transition in a Heisenberg antiferromagnetic linear-chain system[J]. Physical Review Letters, 1975, 35: 744-747.
- [34] INTERRANTE L V, BROWALL K W, HART H R, et al. Preparation and properties of some tetrathiafulvalene donor-acceptor compounds with bis (dithiolene) metal complexes[J]. Journal of the American Chemical Society, 1975, 97(4): 889-890.
- [35] JACOBS I S, BRAY J W, HART H R, et al. Spin-Peierls transitions in magnetic donor-acceptor compounds of tetrathiafulvalene (TTF) with bisdithiolene metal complexes[J]. Physical Review B, 1976, 14: 3036-3051.
- [36] HASE M, TERASAKI I, SASAGO Y, et al. Effects of substitution of Zn for Cu in the spin-Peierls cuprate, CuGeO₃: The suppression of the spin-Peierls transition and the occurrence of a new spin-glass state[J]. Physical Review Letters, 1993, 71: 4059-4062.
- [37] TSUKADA I, TAKEYA J, MASUDA T, et al. Two-stage spin-flop transitions in the $S=1/2$ antiferromagnetic spin chain BaCu₂Si₂O₇ [J]. Physical Review Letters, 2001, 87: 127203.
- [38] HE Z Z, UEDA Y, ITOH M. Magnetic properties of the quasi-one-dimensional system BaMn₂V₂O₈[J]. Solid State Communication, 2007, 141(1): 22-24.
- [39] LÉPINE Y, CAILLÉ A. First order spin-Peierls transition in a quantum antiferromagnetic Heisenberg chain [J]. The Journal of Chemical Physics, 1977, 67(12): 5598-5601.
- [40] CHEN Y, SATO M, TANG Y F, et al. Triplon current generation in solids[J]. Nature Communications, 2021, 12: 5199.
- [41] PARIS E, NICHOLSON C W, JOHNSTON S, et al. Probing the interplay between lattice dynamics and short-range magnetic correlations in CuGeO₃ with femtosecond RIXS[J]. npj Quantum Materials, 2021, 6: 51.
- [42] SUZUKI V Y, AMORIN L H C, DE PAULA N H, et al. New insights into the nature of the bandgap of CuGeO₃ nanofibers: Synthesis, electronic structure, and optical and photocatalytic properties[J]. Materials Today Communications, 2021, 26: 101701.
- [43] XIAO Y M, LI B, QIN L Z, et al. Efficient preparation of CuGeO₃ with controllable morphology using CuCl₂ as copper source[J]. Journal of Inorganic Materials, 2021, 36(1): 69-74.
- [44] XU H Z, ZHANG S Y, GUO G C, et al. Exact dimer phase with anisotropic interaction for one dimensional magnets[J]. Scientific Reports, 2021, 11: 6462.
- [45] VÖLLENKLE H, WITTMANN A, NOWOTNY H. Zur kristallstruktur von CuGeO₃[J]. Monatshefte für Chemie und Verwandte Teile anderer Wissenschaften, 1967, 98: 1352-1357.
- [46] HIROTA K, COX D E, LORENZO J E, et al. Dimerization of Cu-GeO₃ in the spin-Peierls state[J]. Physical Review Letters, 1994, 73: 736.
- [47] HAMAMOTO T, ADACHI N, KIDO G, et al. Phase diagram of spin-Peierls cuprate CuGeO₃ based on ac susceptibility in high magnetic fields[J]. Journal of the Physical Society of Japan, 1994, 63: 1218-1219.
- [48] HORI H, FURUSAWA M, TAKEUCHI T, et al. Magnetic measurements of CuGeO₃ by means of high magnetic field [J]. Journal of the Physical Society of Japan, 1994, 63(1): 18-21.
- [49] KIKUCHI J, YASUOKA H, HASE M, et al. Cu nuclear quadrupole resonance study of CuGeO₃[J]. Journal of the Physical Society of Japan, 1994, 63(3): 872-875.
- [50] KUROE H, KOBAYASHI K, SEKINE T, et al. Heat capacity in an Inorganic spin-Peierls system CuGeO₃ [J]. Journal of the Physical Society of Japan, 1994, 63(1): 365-366.
- [51] HASE M, TERASAKI I, UCHINOKURA K. Observation of the spin-Peierls transition in linear Cu²⁺ (spin-1/2) chains in an inorganic compound CuGeO₃[J]. Physical Review Letters, 1993, 70(23): 3651-3654.
- [52] SUGA S. Two-magnon raman scattering in CuGeO₃ which undergoes spin-Peierls transition [J]. Journal of the Physical Society of Japan, 1993, 62(11): 3829-3831.
- [53] LI Z Q, ZHANG L, SONG Y, et al. Size-controlled synthesis and magnetic properties of copper germanate nanorods. Observation of size-induced quenching of the spin-Peierls transition[J]. CrystEngComm, 2014, 16(5): 850-857.
- [54] TSUKADA I, SASAGO Y, UCHINOKURA K, et al. BaCu₂Si₂O₇: A quasi-one-dimensional $S=1/2$ antiferromagnetic chain system[J]. Physical Review B, 1999, 60(9): 6601-6607.
- [55] LEE P L, HUANG E, KUNG J. High-pressure raman spectroscopy and X-ray diffraction study on scottite, BaCu₂Si₂O₇[J]. Minerals, 2021, 11(6): 608.
- [56] RENDÓN-ANGELES J C, QUIÑONES-GURROLA J R, LÓPEZ-CUEVAS J, et al. Rapid one-pot hydrothermal reaction for preparing BaCu₂Si₂O₇ fine particles with controlled blue colour tonality [J]. Ceramics International, 2021, 47(7): 9354-9365.
- [57] SHIROKA T, EGGENSCHWILER F, OTT H R, et al. From order to randomness: Onset and evolution of the random-singlet state in bond-disordered BaCu₂(Si_{1-x}Ge_x)₂O₇ spin-chain compounds[J]. Physical Review B, 2019, 99: 035116.
- [58] SONG X Q, LU W Z, LOU Y H, et al. Synthesis, lattice energy and microwave dielectric properties of BaCu_{2-x}Co_xSi₂O₇ ceramics [J]. Journal of the European Ceramic Society, 2020, 40(8): 3035-3041.
- [59] SONG X Q, ZOU Z Y, LU W Z, et al. Crystal structure, lattice energy and microwave dielectric properties of melilite-type Ba_{1-x}Sr_xCu₂Si₂O₇ solid solutions[J]. Journal of Alloys and Compounds, 2020,

- 835: 155340.
- [60] WANG G H, XU C Y, CAO H B, et al. Magnetic properties of the low-dimensional $\text{BaM}_3\text{Si}_2\text{O}_7$ system ($\text{M}=\text{Cu}, \text{Co}, \text{Mn}$)[J]. Physical Review B, 2019, 100: 035131.
- [61] ZHANG Z G, MA Q L, BERKE H. Man-made blue and purple barium copper silicate pigments and the pabstite ($\text{BaSnSi}_3\text{O}_9$) mystery of ancient Chinese wall paintings from Luoyang[J]. Heritage Science, 2019, 7: 97.
- [62] KIKUCHI H, FUJII Y, CHIBA M, et al. Experiment observation of the $1/3$ magnetization plateau in the diamond-chain compound $\text{Cu}_3(\text{CO}_3)_2(\text{OH})_2$ [J]. Physical Review Letters, 2005, 94: 227201.
- [63] KIKUCHI H, FUJII Y, CHIBA M, et al. Magnetic properties of the frustrated diamond chain compound $\text{Cu}_3(\text{CO}_3)_2(\text{OH})_2$ [J]. Physica B: Condensed Matter, 2003, 329-333: 967-968.
- [64] KAMIKAWA T, OKUBO S, KUNIMOTO T, et al. High field ESR measurement of diamond chain substance $\text{Cu}_3(\text{OH})_2(\text{CO}_3)_2$ [J]. Physica B: Condensed Matter, 2003, 329-333: 988-989.
- [65] PAL A, ANAND K, YEN T W, et al. Magnetic properties and coupled spin-phonon behavior in quasi-one-dimensional screw-chain compound $\text{BaMn}_2\text{V}_2\text{O}_8$ [J]. Physical Review Materials, 2023, 7: 014402.
- [66] KATSUMATA K, HORI H, TAKEUCHI T, et al. Magnetization process of an $S=1$ linear-chain Heisenberg antiferromagnet [J]. Physical Review Letters, 1989, 63: 86-88.
- [67] LU W, TUCHENDLER J, VON ORTENDERG M, et al. Direct observation of the Haldane gap in NENP by far-infrared spectroscopy in high magnetic fields [J]. Physical Review Letters, 1991, 67: 3716-3719.
- [68] REGNAULT L P, ZALIZNYAK I, RENARD J P, et al. Inelastic-neutron-scattering study of the spin dynamics in the Haldane-gap system $\text{Ni}(\text{C}_2\text{H}_8\text{N}_2)_2\text{NO}_2\text{ClO}_4$ [J]. Physical Review B, 1994, 50: 9174-9187.
- [69] PAHARI B, GHOSHRAY K, SARKAR R, et al. NMR study of ^{51}V in quasi-one-dimensional integer spin chain compound $\text{SrNi}_2\text{V}_2\text{O}_8$ [J]. Physical Review B, 2006, 73: 012407.
- [70] GNEZDILOV V, KURNOSOV V, PASHKEVICH Y, et al. Non-Abelian statistics in light-scattering processes across interacting Haldane chains[J]. Physical Review B, 2021, 104: 165118.
- [71] KURNOSOV V, GNEZDILOV V, LEMMENS P, et al. Phonon excitations in the quasi-one-dimensional Haldane phase of $\text{SrNi}_2\text{V}_2\text{O}_8$ [J]. Low Temperature Physics, 2017, 43(12): 1405-1414.
- [72] TUN Z, BUYERS W J L, HARRISON A, et al. Observation of the Haldane gap in RbNiCl_3 [J]. Physical Review B, 1991, 43: 13331.
- [73] DARRIET J, REGNAULT L P. The compound Y_2BaNiO_5 : A new example of a haldane gap in a $S=1$ magnetic chain[J]. Solid State Communications, 1993, 86(7): 409-412.
- [74] MASLOV S, ZHELUDOV A. Coexistence of Haldane-gap excitations and long-range antiferromagnetic order in mixed-spin nickelates R_2BaNiO_5 [J]. Physical Review B, 1998, 57: 68-71.
- [75] GRANROTH G E, MEISEL M W, CHAPARALA M, et al. Experimental evidence of a Haldane gap in an $S=2$ quasi-linear-chain antiferromagnet[J]. Physical Review Letters, 1996, 77: 1616-1619.
- [76] YOSIDA T, FUKUI M. Crystal structure of $\text{Ni}(\text{C}_3\text{H}_{10}\text{N}_2)_2\text{NO}_2\text{ClO}_4$ [J]. Journal of the Physical Society of Japan, 1992, 61: 2304-2308.
- [77] HASHI K, TSUJII N, SHIMIZU T, et al. NMR evidence for field-induced magnetic ordering at 30 T in the Haldane compound $\text{PbNi}_2\text{V}_2\text{O}_8$ [J]. Journal of the Physical Society of Japan, 2007, 76: 064705.
- [78] PERLEPES S P, BLACKMAN A G, HUFFMAN J C, et al. Complete carboxylate removal from $\text{Mn}_{12}\text{O}_{12}(\text{OAc})_{16}(\text{H}_2\text{O})_4 \cdot 2\text{HOAc} \cdot 4\text{H}_2\text{O}$ with chlorotrimethylsilane: Synthesis and characterization of polymeric (2,2'-bipyridine)trichloromanganate and an improved synthesis of bis (tetraethylammonium) pentachloromanganate(2-)[J]. Inorganic Chemistry, 1991, 30(7): 1665-1668.
- [79] SHINOZAKI S, OKUTANI A, YOSHIZAWA D, et al. Antiferromagnetic order in single crystals of the $S=2$ quasi-one-dimensional chain $\text{MnCl}_3(\text{bpy})$ [J]. Physical Review B, 2016, 93: 014407.